Learning about compact binary merger: The interplay between numerical relativity and gravitational-wave astronomy

Thomas Baumgarte,[1,2] Patrick R. Brady,[3] Jolien D E Creighton,[3] Luis Lehner,[4] Frans Pretorius,[5,6,7] and Ricky DeVoe[8]

[1]*Department of Physics and Astronomy, Bowdoin College, Brunswick, Maine 04011, USA*
[2]*Department of Physics, University of Illinois at Urbana-Champaign, Urbana, Illinois 61801, USA*
[3]*Department Physics, University of Wisconsin-Milwaukee, P.O. Box 413, Milwaukee, Wisconsin 53201, USA*
[4]*Department of Physics and Astronomy, Louisiana State University, Baton Rouge, Louisiana 70810, USA*
[5]*Department of Physics, University of Alberta, Edmonton, Alberta T6G 2G7 Canada*
[6]*Canadian Institute for Advanced Research, Cosmology and Gravity Program, Canada*
[7]*Department of Physics, Princeton University, Princeton, New Jersey 08540, USA*
[8]*Beloit College, 700 College Street, Beloit, Wisconsin 53511, USA*

(Received 22 January 2007; published 11 April 2008)

Activities in data analysis and numerical simulation of gravitational waves have to date largely proceeded independently. In this work we study how waveforms obtained from numerical simulations could be effectively used within the data analysis effort to search for gravitational waves from black hole binaries. To this end we analyze the cross-correlation between different numerical waveforms weighted by the detector's noise. This allow us to propose measures to quantify the accuracy of numerical waveforms for the purpose of data analysis, study how sensitive the analysis is to errors in the waveforms, and propose a way to efficiently encode the waveform's information for its use as a member of the template bank. We estimate that $\sim$100 templates (and $\sim$10 simulations with different mass ratios) are needed to detect waves from *nonspinning* binary black holes with total masses in the range $100M_\odot \leq M \leq 400M_\odot$ using initial LIGO. Of course, many more simulation runs will be needed to confirm that the correct physics is captured in the numerical evolutions. From this perspective, we also discuss sources of systematic errors in numerical waveform extraction and provide order of magnitude estimates for the computational cost of simulations that could be used to estimate the cost of parameter space surveys. Finally, we discuss what information from near-future numerical simulations of compact binary systems would be most useful for enhancing the detectability of such events with contemporary gravitational-wave detectors and emphasize the role of numerical simulations for the interpretation of eventual gravitational-wave observations.

DOI: 10.1103/PhysRevD.77.084009 PACS numbers: 04.30.Db, 04.25.dg

I. INTRODUCTION

Searches for gravitational waves from coalescing compact binary systems rely on concrete knowledge of the waveform to achieve maximum sensitivity to these sources. With LIGO currently acquiring data at design sensitivity (see Fig. 1), an optimal matched filtering search could detect the gravitational waves from binary black hole coalescence out to several hundred Mpc. Direct observation of gravitational waves from these systems will have significant and far reaching consequences for both gravitational physics and astronomy.

To date, searches for gravitational waves from compact binary systems using data taken at LIGO, GEO. and TAMA observatories have concentrated mostly on binary neutron stars and speculative lower mass systems [1]—each element of the binary has a mass below $m_j \leq 3M_\odot$. Searches for inspiral waves from higher mass systems such as binary black holes and black hole neutron star pairs have used detection templates constructed to match with a wide variety of theoretical waveforms [2]. This is the first step in searching for one of the most promising and tantalizing sources accessible to earth-based gravitational-wave detectors. As numerical relativity simulations produce waveforms, new issues arise when trying to migrate this knowledge into analysis efforts.

The gravitational waves measured from a compact binary system depend on a number of parameters including the masses m_1 and m_2, the spins $\vec{s}_1$ and $\vec{s}_2$, the time of merger t_0, and the distance D to the binary. Additional parameters detailing the orbit, specified at some fiducial time, include the inclination of the orbital plane ι relative to the direction to the observer, the eccentricity of the orbit, and the phase of the orbit Φ_0; these are collectively denoted with the symbol Θ. Further, angles describing the location of the binary on the sky and the polarization angle between the propagation and detector frames are needed to obtain the response of a given detector to the incident wave. For binary black holes these are all the free parameters; for neutron stars there are additional parameters that relate to their internal structure and composition. In considering the utility of numerical simulations in gravitational-wave astronomy, it is critical to understand the dependence of the numerical waveforms on all of these parameters. Some of the dependencies are, in principle, in hand already. For example, the functional form of the dependence on sky location, polarization angle, and distance is known analytically if the waves can be extracted

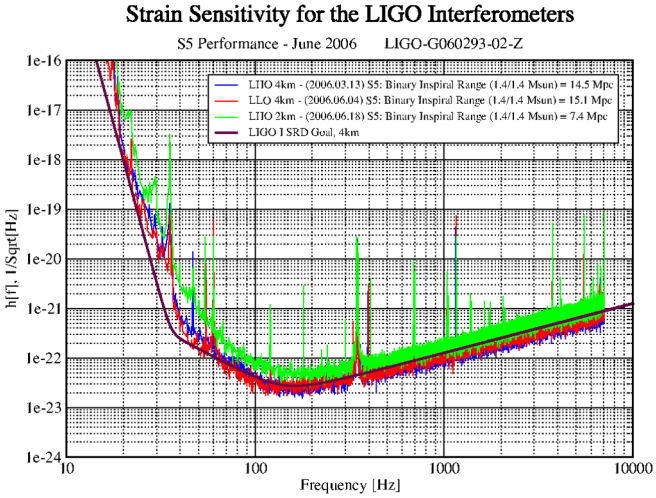

FIG. 1 (color online). The noise sensitivity curves for the LIGO interferometers published in June 2006 [66]. The thick black (blue) and dark grey (red) curves are the 4 km interferometers at Hanford and Livingston, respectively. The light grey (green) curve is the 2 km Hanford interferometer. The LIGO-I noise curve used for the sample calculations in this paper is the thick black (purple) line. Compact binaries generate gravitational waves which sweep upward in frequency as they inspiral and merge. The frequency (≈ 40 Hz) below which the noise curve rises sharply determines the longest dynamical time scale of the sources to which the LIGO instruments are sensitive; this, in turn, translates to a largest mass compact binary system to which LIGO is sensitive.

accurately from numerical simulations. The time of merger is also easily accounted for by translating the computed waveform in time (which is done by applying a frequency dependent phase shift to the waveform).

Post-Newtonian (PN) calculations of the waveforms demonstrate the complicated dependence on the other parameters. When all known amplitude and phase terms are included in the waveform, it is necessary to explicitly measure the masses, spins, inclination, and phase. On the other hand, the so-called restricted post-Newtonian templates (which keep all phase corrections but only the leading amplitude term) provide a simplified and efficient detection method for nonspinning binaries. The data analysis problem (for fixed masses) reduces to the detection of a signal of unknown amplitude and phase for which the optimal method is well known [3].

In this paper, we present preliminary investigations of waveform accuracy and discuss implications for numerical simulations. In Sec. II, we give an overview of the form of the gravitational-wave strain that is measured at detectors, the relationship between this and a common way of describing the waveform from numerical simulations in terms of Weyl scalars, and summarize the numerical results we will use as examples. In Sec. III, we provide a framework to obtain an estimate of the accuracy of a particular simulation with relation to the data analysis techniques. We present examples from the perspective of both inspiral and burst searches, and from the inspiral study we obtain a crude estimate that, for the purposes of *detection* of *nonspinning* binaries, a template bank for initial LIGO containing approximately 100 waveforms will be sufficient; this corresponds to about 10 simulations with different mass ratios. In Sec. IV, we conclude with broad discussions of several important and related issues, including certain technical aspects of waveform extraction from simulations that might introduce spurious effects—details of this discussion are deferred to Appendix A. We also explain how information from current simulations, before fully qualified simulations can produce template waveforms, can be used to enhance the detection of binary black holes using excess-power type searches tuned to the right frequencies. Finally, we discuss how numerical simulations may be used to interpret eventual gravitational-wave observations. Most of our analysis focuses on binary black hole systems, although in Sec. IV we also comment on other compact binaries that contain one or two neutron stars. In Appendix B we provide scaling estimates of the CPU time (cost) required to simulate binary systems. This should be useful to estimate how feasible various surveys of binary black hole merger parameter space would be on contemporary computer systems.

II. GRAVITATIONAL WAVEFORMS FROM BLACK HOLE BINARIES

For a binary black hole system, the gravitational-wave strain measured at one of the detectors can be written as

$$h(t) = F_+(\alpha, \delta, t, \psi) h_+(t - t_0; m_1, m_2, \vec{s}_1, \vec{s}_2, D, \Theta) + F_\times(\alpha, \delta, t, \psi) h_\times(t - t_0; m_1, m_2, \vec{s}_1, \vec{s}_2, D, \Theta), \tag{1}$$

where m_1 and m_2 are the black hole masses, $\vec{s}_1$ and $\vec{s}_2$ are the black hole spins, t_0 is the time of merger, D is the distance to the binary, (α, δ) are the right ascension and declination of the binary, ψ is the polarization angle between the propagation and detector frame, and Θ includes the various elements needed to uniquely specify the orbit—for small spins and circular orbits these elements are the inclination of the orbital plane, ι, and the phase of the orbit at time of merger, Φ_0.

Numerical waveforms are usually obtained from the Weyl scalar Ψ_4. Under a careful choice of coordinates, frame, and extraction world tube (further discussion of which is presented in Sec. IV and Appendix A), the waveform is related to Ψ_4 by

$$\frac{d^2}{dt^2}(h_+ + i h_\times) = \Psi_4. \tag{2}$$

It is often convenient to represent the waveform in terms of spin-weight -2 spherical harmonics as

$$h_+ + ih_\times = \sum c_{lm-2} Y_{lm}. \quad (3)$$

For concreteness, we consider waveforms extracted from numerical simulations performed by Pretorius [4]; similar calculations can certainly be done with waveforms extracted from other simulations [5–10].

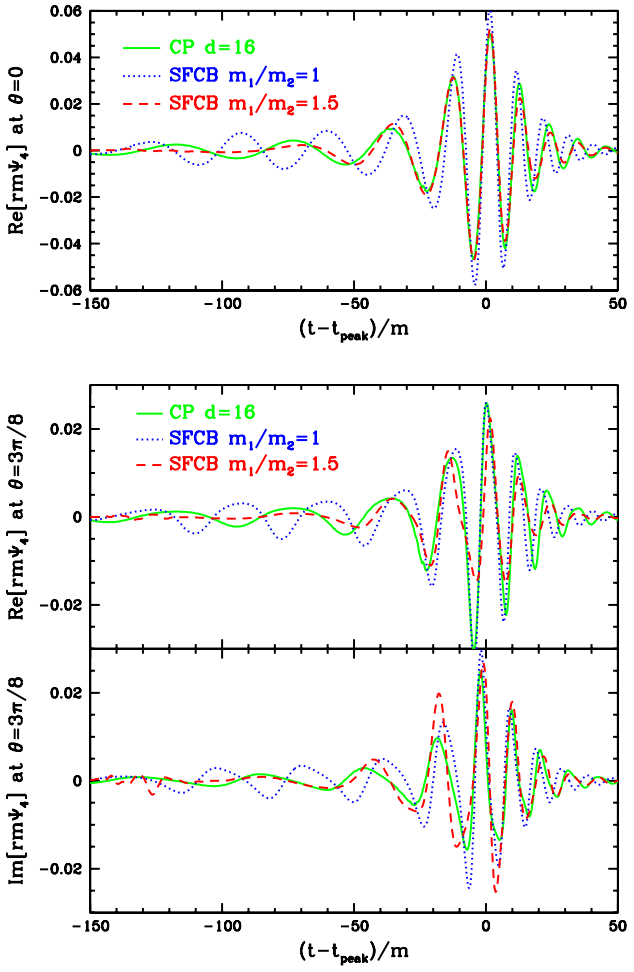

FIG. 2 (color online). Samples of Ψ_4 from the binary black hole merger simulations discussed here. Evolutions from three different initial conditions are shown: Cook-Pfeiffer $d = 16$ (CP d = 16), and two scalar field collapse binaries, one equal mass, the other with a mass ratio of 1.5:1. The top plot shows the real part of Ψ_4 evaluated along the axis $\theta = 0$ orthogonal to the orbital plane (and azimuthal angle $\phi = 0$); for brevity we do not show the imaginary part as it looks almost identical modulo a phase shift. The figures below show the real and imaginary parts of Ψ_4 evaluated at $\theta = 3\pi/8$ (note the different vertical scale). Here we show both components as there are noticeable differences between the two polarizations. In all cases the waveform was extracted at a coordinate radius of $r = 50m$, where m is the sum of initial apparent horizon masses; also, the time has been shifted so that $t = 0$ corresponds to the peak in wave amplitude, and Ψ_4 has been multiplied by a constant complex phase angle to aid comparison.

The simulations evolve two classes of initial data: (a) - equal-mass, quasicircular corotating initial configurations as calculated by Cook and Pfeiffer [11–13], and (b) black hole binary systems formed via the gravitational collapse of two boosted scalar field pulses. A detailed analysis of the Cook-Pfeiffer (CP) evolutions is presented in [14]. The scalar field collapse binaries (SFCB) have nonnegligible initial eccentricity, zero initial spin, and simulations with mass ratios up to 1.5:1 have been performed (a more detailed description of the equal-mass scenarios can be found in [4,15]). Note that the scalar field is merely a convenient vehicle to create binary configurations; remnant scalar field energy leaves the vicinity of the binaries in about one light crossing time (on the order of 1/4 orbit) and is dynamically insignificant for the subsequent evolution of the binary, and, in particular, the gravitational waves that are generated. Here we study three examples from these evolutions—a CP $d = 16$ case (d labels the initial separation between the binaries [11]) and two SFCBs, one equal mass, the other with a mass ratio of 1.5:1. The two former evolutions exhibit roughly 2.5 orbits before merger, the latter unequal mass case about 1.5 orbits. In all cases the remnant is a Kerr black hole with spin parameter $a \approx 0.7M_f$, where M_f is the final mass of the black hole, and roughly 3%–5% of the initial mass energy (i.e. the sum of the individual masses in the initial data) of the system is radiated away in gravitational waves. Figure 2 shows a few samples of the waveforms extracted from these simulations, while Fig. 3 demonstrates the convergence behavior of the wave with resolution for the CP case. In Fig. 2, data from the highest resolutions available are shown.

Observe that the waveforms depicted in Fig. 2 have some noticeable differences. By construction the phases all match at $t = 0$. On axis, the CP and unequal mass

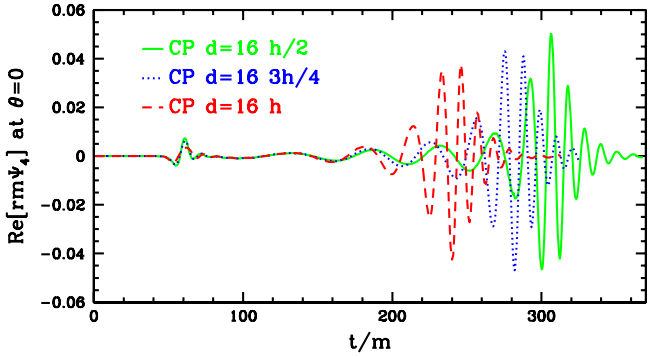

FIG. 3 (color online). A plot demonstrating the dependence on numerical resolution of Cook-Pfeiffer $d = 16$ initial data evolutions. The lowest characteristic resolution (dashed line) has a characteristic mesh spacing of h, the next lowest one of $3h/4$ (dotted line), while the finest resolution has a mesh spacing of $h/2$ (solid line). The dominant component of the numerical error is in the phase evolution of the inspiral portion of the wave. See [14] for a detailed discussion of the numerical errors in this set of evolutions.

SFCBs have similar phase and amplitude evolution of the waveform several cycles to the left and right of $t = 0$; however, moving toward the orbital plane the similarities are less evident. There is also a more rapid decoherence between the equal-mass SFCB and the other two cases moving away from $t = 0$. One reason for this is that the equal-mass SFCB example has initial conditions tuned to exhibit some ''zoom-whirl'' type behavior, showing a couple of whirl orbits before the system finally merges. During the whirl phase the binaries are quite close together [inside of what might be considered an innermost stable circular orbit (ISCO)] and moving faster than a corresponding point in a quasicircular inspiral. Hence the amplitude of this portion of the wave is quite a bit larger than the quasicircular case and remains similar in magnitude over a couple of wave cycles. These differences are in contrast to quasicircular equal-mass inspiral results obtained by most groups, visual comparisons of which suggest remarkable similarity in the waveforms over several wave cycles away from the matching point [16,17]. Given that *all* the latter evolutions are approximations to *essentially the same* astrophysical scenario, the similarity is not too surprising, but nevertheless is reassuring.

It is also interesting to examine the Fourier spectrum of these waveforms and to notice the similarities and differences that are manifest. The amplitude of the Fourier transform of the gravitational waveform, from the evolution of Cook-Pfeiffer initial data, shown in Fig. 2, is plotted in Fig. 4. This is computed directly from $\Psi_4(t)$ using the frequency domain equivalent of Eq. (2) which gives, for example,

$$-4\pi^2 f^2 \tilde{h}_+(f) = \tilde{\Psi}_4^R(f), \tag{4}$$

where $\tilde{\Psi}_4^R(f)$ and $\tilde{h}_+(f)$ are the Fourier transform of the real part of Ψ_4 and the strain, respectively (see Sec. III A). This avoids introducing artifacts from the numerical inte-

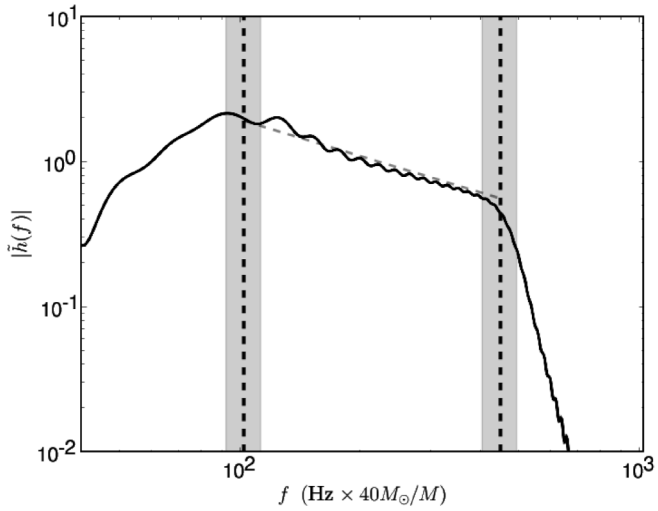

FIG. 4. The amplitude of the Fourier transform of the gravitational waveform, from the evolution of Cook-Pfeiffer initial data, shown in Fig. 2. The vertical dashed lines are the estimated frequency of the inner-most stable circular orbit given in Eq. (5) and the frequency of the dominant quasinormal mode, assuming $a = 0.7M_f$, given in Eq. (6). The gray shaded region indicates variations in this frequency due to 10% changes in the mass used. Notice how the power in these waves is predominantly emitted between these two frequencies; the initial data is such that the binary is orbiting at or near the ISCO frequency. In addition, the dashed gray line which follows the amplitude is proportional to $f^{-5/6}$. While this is a convincing fit to the amplitude, we note that there is weak evidence for two power laws $f^{-7/6}$, as given by post-Newtonian approximations [67], below $\sim 1.5 f_{\rm isco}$ and $f^{-5/6}$ above that frequency. These simulations do not cover the inspiral phase well enough to confirm this result.

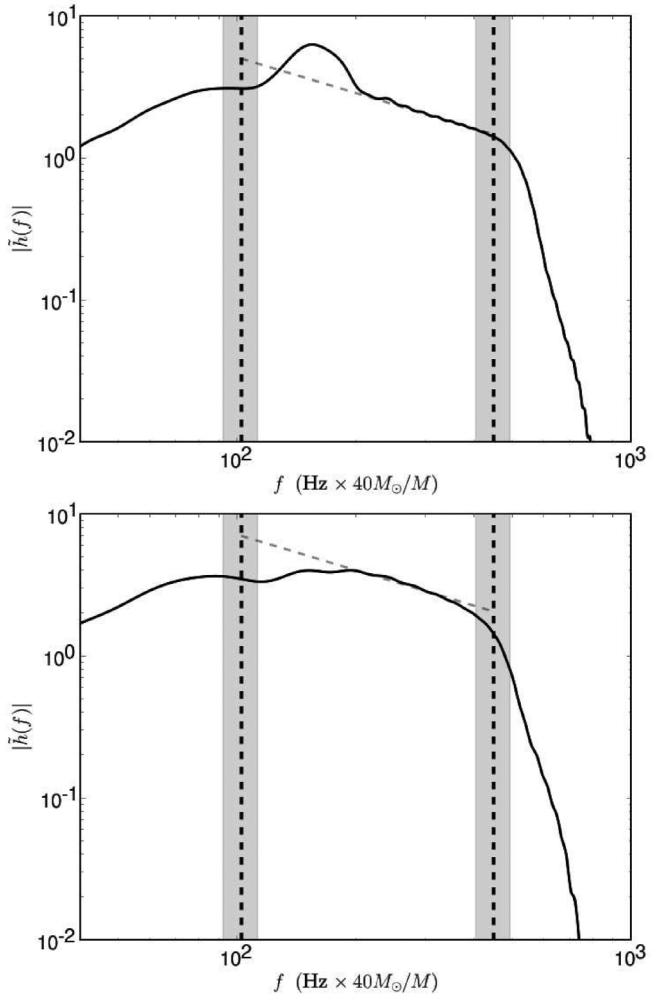

FIG. 5. The amplitude of the Fourier transform of the gravitational waveforms shown in Fig. 2: the top panel is an equal-mass SFCB, and the lower panel is a mass ratio 1.5:1 SFCB. Note the differences between these spectra and that shown in Fig. 4. The bump in the equal-mass spectrum arises from the hangup of the binary at roughly constant separation with a brief whirl phase prior to merger.

gration of Eq. (2). To guide the eye, we indicate the frequency of the innermost stable circular orbit estimated by Kidder *et al.* [18]

$$f_{\rm isco} \approx 205\left(\frac{20.0M_\odot}{M}\right)\ {\rm Hz}, \tag{5}$$

and the frequency of the $l = m = 2$ mode of quasinormal ringing given by

$$f_{\rm qnr} \approx 1600[1 - 0.63(1.0 - a)^{0.3}]\left(\frac{20M_\odot}{M_{\rm BH}}\right)\ {\rm Hz}, \tag{6}$$

where M is the total mass of the binary, and $M_{\rm BH}$ and a are the mass and spin of the final black hole. Notice how the power in these waves is predominantly emitted between these two frequencies–the initial data is such that the binary is orbiting at or near the ISCO frequency. Moreover, the spectrum shows a power-law spectrum reminiscent of the behavior of post-Newtonian waveforms. Similar plots are shown in Figs. 5 for the SFCB waveforms. It is interesting to note the bump in the spectrum when $m_1 = m_2$; this appears to be caused by the zooming orbits referred to above. It points to the variety of waveform morphologies that might exist for binary black hole mergers when eccentricity and even spin of the black holes is large.

The preceding discussion of similarities and differences between waveforms is quite heuristic and subjective, and thus of arguable merit. One of the main purposes of this paper is to propose metrics to both quantify the accuracy of simulations and the similarities/differences between waveforms, though primarily from the perspective of data analysis. The sets of waveforms depicted in Figs. 2 and 3, that *appear* to be significantly different due to either numerical resolution effects or different initial physics parameters, will provide useful test cases to gauge the efficacy of the proposed metrics.

III. ESTIMATING THE WAVEFORM ACCURACY

The accuracy of numerical solutions is generally determined by comparing results obtained at different grid resolutions (and at different boundary locations if these are not placed sufficiently far away to ensure they are causally disconnected from the region of interest). This approach determines the pointwise convergence of the solutions. In the context of gravitational-wave astronomy, only the waveforms themselves are directly accessible to observation. It is therefore important, if the results of numerical simulations are to be useful to gravitational-wave astronomers, to provide a measure of the waveform accuracy.

A. Data analysis formalism

The standard tool of gravitational-wave data analysis is the matched filter. If a signal is present, the detector output is

$$s(t) = n(t) + h(t; \hat{\lambda}), \tag{7}$$

where $n(t)$ is the noise and $h(t; \hat{\lambda})$ is the signal. In general, the signal depends on a set of unknown (in advance) parameters $\hat{\lambda}$. We assume the noise is a zero mean $\langle n(t)\rangle = 0$ and stationary process, i.e. $\langle n(t)\rangle = 0$ and $\langle n(t_1)n(t_2)\rangle = Q(|t_1 - t_2|)$ for some function Q. Here $\langle \ldots \rangle$ denotes the ensemble average over different instantiations of the noise.

Define the Fourier transform of the noise by

$$\tilde{n}(f) = \int_{-\infty}^{\infty} n(t)e^{-2\pi i f t}dt. \tag{8}$$

Since the Fourier transform is just a linear transformation of the noise time series, we also have $\langle \tilde{n}(f)\rangle = 0$. Further, the variance or power spectrum $S_n(|f|)$ is defined by

$$\langle \tilde{n}(f)\tilde{n}^*(f')\rangle = \tfrac{1}{2}S_n(|f|)\delta(f - f'). \tag{9}$$

Notice that this two point function is diagonal; this is a direct consequence of the stationarity of the noise. Moreover, the power spectrum of the noise will depend nontrivially on frequency if the time-domain correlation function is not diagonal. Noise with a frequency dependent power spectrum is often referred to as colored noise.

In its simplest form, matched filtering is cross-correlating a template waveform $w(t; \lambda)$ with the time series $s(t)$ observed by the gravitational-wave detector. The matched filter signal-to-noise ratio (SNR) is

$$\rho(\lambda) = \frac{2}{\sigma_w}\int_{-\infty}^{\infty} df \frac{\tilde{s}(f)\tilde{w}^*(f; \lambda)}{S_n(|f|)}, \tag{10}$$

where

$$\sigma_w^2 = 2\int_{-\infty}^{\infty} df \frac{\tilde{w}(f; \lambda)\tilde{w}^*(f; \lambda)}{S_n(|f|)}. \tag{11}$$

Notice that the signal-to-noise ratio is normalized such that $\langle \rho^2\rangle = 1$ if the signal is absent, i.e. $h(t; \hat{\lambda}) \equiv 0$.

Since the signal parameters are not known in advance, one must search over all possible values of the parameters λ to find the template that best matches the signal buried in the noise. Then the output of a search (over a small chunk of data) will be

$$\rho = \max_{\lambda} \rho(\lambda). \tag{12}$$

The largest SNR will be obtained when $w(t; \lambda) =$ constant $\times\, h(t; \hat{\lambda})$ and $\lambda = \hat{\lambda}$. In practice, two important issues arise. First, only a discrete set of values of λ can be searched. This leads to the notion of a bank of templates with different parameter values. There is a well-developed formalism for constructing template banks [19] for gravitational-wave data analysis. In Sec. III D, we will comment on the number of templates needed for the binary black hole problem and hence the number of accurate numerical simulations that must be done. Second, the

theoretical template waveforms may not accurately agree with the real signals. It is this issue which we address here.

The expected SNR is then

$$\langle \rho(\lambda) \rangle = \frac{2}{\sigma_w} \int_{-\infty}^{\infty} df \frac{\tilde{h}(f;\hat{\lambda}) \tilde{w}^*(f;\lambda)}{S(|f|)}. \tag{13}$$

If the template and the signal are the same, then the optimal SNR (squared) is

$$\langle \rho_{\rm opt} \rangle^2 = \sigma_h^2 = 2 \int_{-\infty}^{\infty} df \frac{|\tilde{h}(f;\hat{\lambda})|^2}{S_n(|f|)}. \tag{14}$$

Define the match [19] between a waveform and a template by

$$\mu = \frac{\langle \rho(\lambda) \rangle}{\langle \rho_{\rm opt} \rangle} \tag{15}$$

$$= \frac{2}{\sigma_h \sigma_w} \int_{-\infty}^{\infty} df \frac{\tilde{h}(f;\hat{\lambda}) \tilde{w}^*(f;\lambda)}{S(|f|)}. \tag{16}$$

The *fitting factor* [20]

$$\mathrm{FF} = \max_{\lambda} \mu \tag{17}$$

is a measure of the distance between a signal and the whole template space. If FF = 1, the signal lies inside the template space. We will generally use the term match to mean something that is maximized over a subset of the parameters λ and keep the fitting factor for the case when all template parameters have been maximized over.

B. Reparametrization of the numerical templates

In general, the response of a gravitational-wave detector to the waves from a compact binary merger will be nontrivial as expressed in Eq. (1). Motivated by our intuitive expectation that gravitational radiation is dominated by the quadrupole waves, we have explored the following reparametrization of the numerical waveforms:

$$w(t;\lambda) \approx A \left(\frac{1\ \mathrm{Mpc}}{D} \right) [\cos\Phi \hat{e}_+(t - t_0; m_1, m_2) + \sin\Phi \hat{e}_\times(t - t_0; m_1, m_2)], \tag{18}$$

where A and Φ depend on the right ascension α, declination δ, polarization ψ, inclination ι, and time t. (The variation in these constants over the short duration of the signal is completely negligible; however, the response of the instrument to a gravitational wave from a given location on the celestial sphere depends on the time of day.) Here the plus and cross polarization states $\hat{e}_{+,\times}(t - t_0; m_1, m_2)$ are just the waveforms extracted on the axis orthogonal to the plane of the binary orbit. Explicitly, $\hat{e}_+(t - t_0; m_1, m_2) + i\hat{e}_\times(t - t_0; m_1, m_2) = c_{2,2}(t - t_0; m_1, m_2, D = 1\ \mathrm{Mpc})$ with $c_{2,2}$ being the $l = m = 2$ mode in the expansion given by Eq. (3). Here we present evidence that this reparametrization may capture the essential features of the merger waveforms sufficiently well for the purposes of detecting the waves. On the other hand, the full waveforms will probably be needed to extract all the possible science.

To see that this approximation is good enough for detection, we reexpress the matched filtering SNR in terms of these templates. First, notice that the amplitude $A \times (1\ \mathrm{Mpc}/D)$ cancels out of the SNR defined in Eq. (10). Hence the SNR can be expressed as

$$\rho = \max_{\Phi, t_0, m_1, m_2} \frac{z_+ \cos\Phi + z_\times \sin\Phi}{\bar{\sigma}_w}, \tag{19}$$

where $\bar{\sigma}_w = D\sigma_w/(A \times 1\ \mathrm{Mpc})$ and

$$z_{+,\times}(t_0; m_1, m_2) = 2 \int_{-\infty}^{\infty} \frac{\tilde{s}(f) \tilde{e}^*_{+,\times}(f; m_1, m_2)}{S_n(|f|)} e^{2\pi i f t_0} df. \tag{20}$$

For the waveforms considered here, we find that

$$2 \int_{-\infty}^{\infty} df \frac{|\tilde{e}_+(f; m_1, m_2)|^2}{S_n(|f|)} \approx 2 \int_{-\infty}^{\infty} df \frac{|\tilde{e}_\times(f; m_1, m_2)|^2}{S_n(|f|)} \tag{21}$$

to better than 3% accuracy. We also find that the two polarizations are almost orthogonal, that is

$$\int_{-\infty}^{\infty} df \frac{\tilde{e}_+(f; m_1, m_2) \tilde{e}^*_\times(f; m_1, m_2)}{S_n(|f|)} \approx 0, \tag{22}$$

with typical values $\sim 3 \times 10^{-3}$. Hence the normalization constant σ_w simplifies considerably and is independent of Φ and t_0:

$$\sigma_w^2 \approx \sigma_e^2 = 2 \int_{-\infty}^{\infty} df \frac{|\tilde{e}_+(f; m_1, m_2)|^2}{S_n(|f|)}. \tag{23}$$

This allows us to maximize over Φ analytically to find

$$\rho = \max_{t_0, m_1, m_2} \sigma_w^{-1} \sqrt{z_+^2(t_0; m_1, m_2) + z_\times^2(t_0; m_1, m_2)}. \tag{24}$$

Below, we will use the plus and cross quadrature matched filters to quantify both the accuracy of the numerical simulations and the accuracy of the approximation introduced in Eq. (18).

Moreover, the match can be written as

$$\mu = \max_{\Phi, t_0, m_1, m_2} (\mu_+ \cos\Phi + \mu_\times \sin\Phi) \tag{25}$$

where

$$\mu_{+,\times} = \frac{\langle z_{+,\times} \rangle}{\sigma_h \sigma_e}. \tag{26}$$

It is straightforward to see that the validity of the reparametrization in Eq. (18) requires that $\mu_+ \approx 1$ and $\mu_\times \approx 0$, independent of the inclination ι, when $h(t, t_0, m_1, m_2) = h_+(t, t_0, m_1, m_2, \iota)$, and that $\mu_\times \approx 1$ and $\mu_+ \approx 0$, inde-

TABLE I. The range of matches between waveforms extracted at different angles relative to the binary and a template given by the waveform extracted at the axis for masses $40M_\odot < M < 200M_\odot$. The inclination, ι, is the angle between the orbital angular momentum vector and the direction from the source to the observer. Note that the $++$ and $\times\times$ entries are all very close to unity. The $+\times$ entries are close to zero indicating that the $+$ and $\times$ polarizations are almost orthogonal. This suggests that the reparametrization in Eq. (18) could be good enough for detection purposes, with LIGO, in the equal-mass binary case.

CP	$h_+(t_0, m_1, m_2, \iota)$		$h_\times(t_0, m_1, m_2, \iota)$	
ι	$3\pi/8$	$\pi/4$	$3\pi/8$	$\pi/4$
μ_+	[0.980,0.995]	[0.990,0.996]	[0.017,0.044]	[0.044,0.066]
$\mu_\times$	[0.050,0.074]	[0.046,0.069]	[0.989,0.995]	[0.992,0.996]

SFCB	$h_+^{\mathrm{SFCB}}(t_0, m_1 = m_2, \iota)$		$h_\times^{\mathrm{SFCB}}(t_0, m_1 = m_2, \iota)$	
ι	$3\pi/8$	$\pi/4$	$3\pi/8$	$\pi/4$
μ_+	[0.981,0.989]	[0.993,0.996]	[0.021,0.044]	[0.019,0.032]
$\mu_\times$	[0.051,0.075]	[0.024,0.038]	[0.995,0.989]	[0.995,0.998]

SFCB	$h_+^{\mathrm{SFCB}}(t_0, m_1 = 1.5m_2, \iota)$		$h_\times^{\mathrm{SFCB}}(t_0, m_1 = 1.5m_2, \iota)$	
ι	$3\pi/8$	$\pi/4$	$3\pi/8$	$\pi/4$
μ_+	[0.969,0.973]	[0.986,0.991]	[0.042,0.056]	[0.040,0.050]
$\mu_\times$	[0.076,0.096]	[0.049,0.061]	[0.987,0.977]	[0.989,0.993]

pendent of the inclination ι, when $h(t, t_0, m_1, m_2) = h_\times(t, t_0, m_1, m_2, \iota)$. This result is confirmed in Table I; only the mass space needs to be searched by the explicit construction of a discrete bank of templates.

It must be stressed, however, that this approach is not sufficient for the interpretation of observations and measurement of parameters. Moreover, there are likely to be regimes where this approach is insufficient even for detection.

C. Example of waveform accuracy estimation

As we mentioned above, differences between the true waveform from a binary black hole merger and the template waveform can result in degradation of the SNR. In particular, numerically generated waveform templates might be inaccurate for any number of reasons, e.g. truncation errors, instabilities, errors in boundary conditions, or incorrect waveform extraction. To get a handle on these effects, it is useful to compare waveforms which are supposed to represent the same physical process that were generated in different ways.

Here, we present a sample analysis of the waveforms presented in [4,14,15]. Using the formalism outlined above, one can compute the matches μ_+ and $\mu_\times$ for the waveform generated at the finest resolution and templates at coarser resolutions. This investigation follows the standard convergence testing of numerical relativity, but with an emphasis on the utility of the waveforms for data analysis. Moreover, the answer to this question depends on the mass of the binary and the detector being considered (as it depends on its particular noise curve). In Fig. 6, we show the match μ_+ versus the binary mass for the initial LIGO noise curve shown in Fig. 1. For each template waveform (i.e. the waveforms from evolutions with coarser resolution), there are sets of points: the triangles indicate the match before maximization over t_0, the circles indicate the match after maximization over t_0. When the match exceeds 0.9, we may be tempted to conclude that the finest resolution waveforms are sufficiently accurate to be used for gravitational-wave data analysis. This is not the whole story, however. Referring back to Fig. 4, we note that the waves with frequencies $f \lesssim 205(20M_\odot/M)$ appear to depend on the initial data while those above that frequency might reasonably be considered independent of the initial data. Given that the current LIGO instruments are sensitive to waves above 40 Hz, this suggests that the match should only be trusted for masses $M \gtrsim 100M_\odot$.

On the other hand, the small match obtained without maximization over time suggests that the evolutions are slightly different. In Fig. 7, we show the time shift needed to maximize the match. Note that the shift scales linearly with mass. This suggests that the difference between these waveforms might be captured simply by rescaling the mass of the template, i.e. maximizing over both total mass and time delay as one would do in a search. In a simple simulation which searched over various template masses for a fixed waveform mass, it was found that the best match is achieved when the template mass is different from the

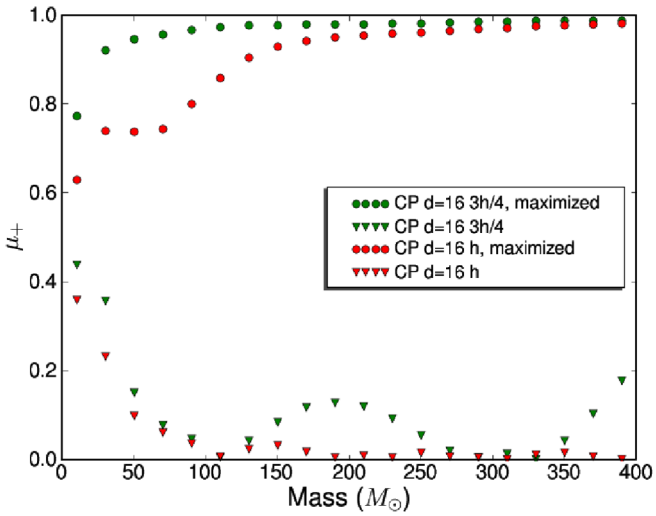

FIG. 6 (color online). The match between the h_+ waveform polarization computed as the overlap between the waveforms extracted from two different resolution runs. Circles indicate the match when the waveforms are allowed to shift in time relative to each other. The triangles indicate the match computed as the overlap integral between waveforms without the time shift. The highest resolution simulation is used as the reference and the match with two coarser resolution simulations are computed.

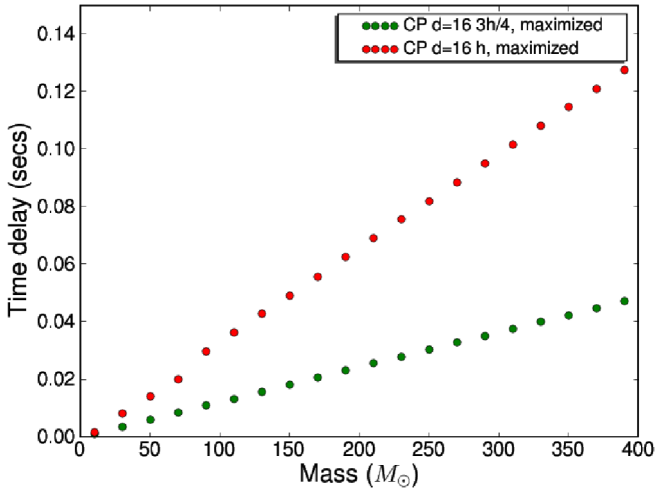

FIG. 7 (color online). The time-offset which maximizes the match (for the same mass) between the h_+ waveform polarization computed as the overlap between the waveforms extracted from two different resolution runs. The bottom (green) uses the finest simulation as the waveform and the coarsest simulation as the template; the top (red) uses the finest simulation as the waveform and the next finest simulation as the template.

waveform mass, but the time shift is similar in magnitude to that obtained when using the same mass in both the template and the waveform.

In this concrete example, we have compared the waveforms from the same simulation at different resolutions. While the waveforms generated at the finest resolution appear to be accurate enough to use as templates in searches for gravitational waves, the systematic differences between the mass and t_0 which maximizes the match hint that the waveforms may not be faithful to the physical system. That is, the map between mass of the template and mass of the binary (in the standard Newtonian sense) may have systematic biases. It will be important to explore these issues by comparing waveforms from simulations (starting from the same initial data) by different groups. Moreover, detailed exploration of the dependence of the waveforms on the initial data will also bring information about the faithfulness of the waveforms [21].

D. Comparing waveforms from different simulations

In the previous section, we presented a comparison between waveforms extracted from simulations at different resolutions in order to gain insight into the accuracy of the numerical solutions. Another important step in exploring the full parameter space of compact binary inspiral for earth-based detectors is to compare the results of different simulations. There are two different reasons for making these comparisons: First, comparison of waveforms representing the same physical solution carried out using different methods will allow a deeper understanding of the numerical issues in this very complicated simulation problem. Second, it may allow more efficient exploration of the parameter space if multiple groups can agree on some key test cases and then explore, in detail, other regions of parameter space.

As an example, we compare the waveforms from the CP simulations with those from the SFCB simulations and between the different SFCB simulations in Fig. 8. The results quantify the degree to which these waveforms are different/similar as seen in Figs. 2–5. For example, the match (maximized over time and phase) between $h_+^{\rm CP}$ and the equal-mass SFCB waveforms is greater than 0.95 for masses $M \gtrsim 200.0 M_\odot$. This is consistent with agreement in both frequency spectrum [$f \gtrsim 200(40 M_\odot/M)$] and the waveform. The biggest difference between these waveforms therefore appears to come from the eccentricity of the binary orbit when the black holes first form in SFCBs. A similar conclusion holds for the match (maximized over time and phase) between $h_+^{\rm SFCB}(m_1 = m_2)$ and the SFCB waveform for mass ratio $m_1/m_2 = 1.5$.

Finally, we note that the number of templates needed to *search* for gravitational waves from *nonspinning binaries in data from earth-based detectors* can be estimated as follows. From the CP simulations, we find that the match (maximized over time and phase) is $\mu \geq 0.97$ for two waveforms with masses differing by $\approx 0.05M$ with $100 M_\odot < M < 400 M_\odot$. Templates along the equal-mass line would then be laid out with separations $\approx 0.1M$ giving $\approx \int_{100}^{400} dM/(0.1M) \approx 14$ templates. If we construct a square grid on the $m_1 m_2$-space by drawing lines through the equal-mass template points, this gives ≈ 105 templates to cover the square defined by $50 M_\odot < m_1, m_2 < 200 M_\odot$. This formula assumes a maximum reduction in SNR of 3%

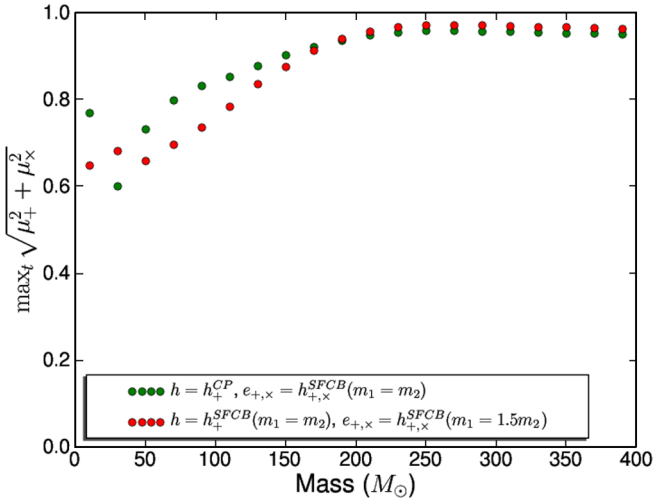

FIG. 8 (color online). The match between the h_+ waveform polarization from one simulation with the waveforms from another simulation maximized over both time and phase. The match $\max_t \sqrt{\mu_+^2 + \mu_\times^2} \gtrsim 0.95$ for masses $M \gtrsim 200 M_\odot$. This gives a quantitative measure of the similarities and differences between the waveforms presented in Figs. 2–5.

due to template mismatch. Since a single numerical simulation gives all templates along a line of constant mass ratio, this suggests that about 10 simulation runs would be needed to cover this mass space densely enough for detection purposes. This crude estimate should be refined with more detailed simulations with different mass ratios and larger initial separations. It is important to stress here that this number assumes that all the physics and numerical issues are under complete control, that no tuning or test runs need to be made, and that the waveforms do not get much more complicated as the mass ratio changes. All of these issues need to be explored before one could generate waveform templates that could be confidently used in gravitational-wave detection. As a result, while the final number of templates is not very large, reaching the stage where these runs can be made requires much greater effort.

It is important not to read too much into the estimate stated above. As we have emphasized, it ignores spin and many other important issues in numerical relativity. It is also only applicable to earth-based detectors. The problem is different for higher mass binaries in the LISA (Laser Interferometer Space Antenna) band. Finally, it only estimates the number of simulations needed to enhance detection. As we discuss later, this is the first step in using numerical methods to extract scientific information from gravitational-wave observations, but the larger computational task will be extracting accurate information from the data once a detection is made.

E. Detectability of numerical templates using ringdown filters

It is illustrative to determine how well existing methods of searching for gravitational-wave bursts would work in detecting numerical waveforms. In particular, we would expect that ringdown waveform matched filters would work well at detecting the end of the numerical waveforms (which do correspond to black hole quasinormal mode ringdown)—especially if it is this portion of the waveform that is in the detector band. However, for a broad range of masses it is the merger waveform that is in LIGO's sensitive band rather than the ringdown waveform: indeed, for the most likely ranges of binary black hole masses, the ringdown radiation will be at frequencies higher than the most sensitive portion of LIGO's band. Nevertheless, the numerical waveforms might be well matched by a ringdown template even at frequencies below those of the final black hole's quasinormal mode. Will a ringdown matched filter template actually do well at detecting these numerical waveforms? Also, will the presence of a preceding waveform bias ringdown extraction parameters? The answer to both of these questions seems to be yes.

The match, μ, can be used to measure the ability of the ringdown filter to detect the waveform. In the case of a ringdown filter the relevant parameters that we must maximize in forming the match are the start time of the ringdown t_0, the central frequency of the ringdown f_0, and the ringdown quality factor Q which measures the decay time of the ringdown in cycles. A ringdown waveform is an exponentially damped sinusoid: $\exp(-\pi f_0 \tau/Q) \times \cos(2\pi f_0 \tau)$ for $\tau = t - t_0 > 0$. As before, the match is an indication of the fraction of the signal-to-noise ratio that a ringdown filter will obtain compared to an optimal filter. The match will depend on the mass of the waveform as this determines which portion of the waveform is in LIGO's band. From Fig. 4 it can be seen that the numerical waveforms do not accurately give the gravitational-wave energy below 40 Hz for a $100M_\odot$ black hole. Since 40 Hz is roughly the low-frequency bound of LIGO's sensitive band, care must be taken in interpreting the match when using low mass waveforms with a total mass less than $\approx 100M_\odot$ since a substantial contribution to the gravitational-wave signal is missing in LIGO's sensitive band.

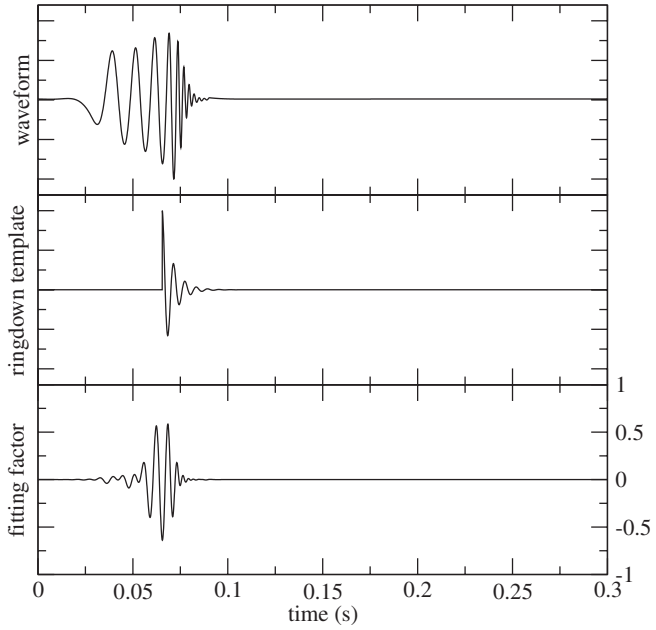

FIG. 9. The h_+ numerical waveform for a total mass of $50M_\odot$ (top), the best-matching ringdown (exponentially damped sinusoid) filter (middle), and the result of filtering the waveform with this filter (bottom), all as functions of time. The match, which is the largest absolute value of the bottom plot, is 64%. The best match clearly occurs before what we would call the ringdown phase of the numerical simulation: this is because the ringdown phase is not in LIGO's sensitive band for a total mass of $50M_\odot$—the ringdown filter therefore obtains its best match at an earlier (and lower frequency) portion of the numerical waveform. Although the ringdown filter does not do too badly at detecting the numerical waveform, it could not be used to measure the quasinormal mode frequency of the final black hole without using information from both the ringdown and merger phases. This serves to emphasize the importance of developing data analysis techniques which combine information from all three phases of binary evolution [68].

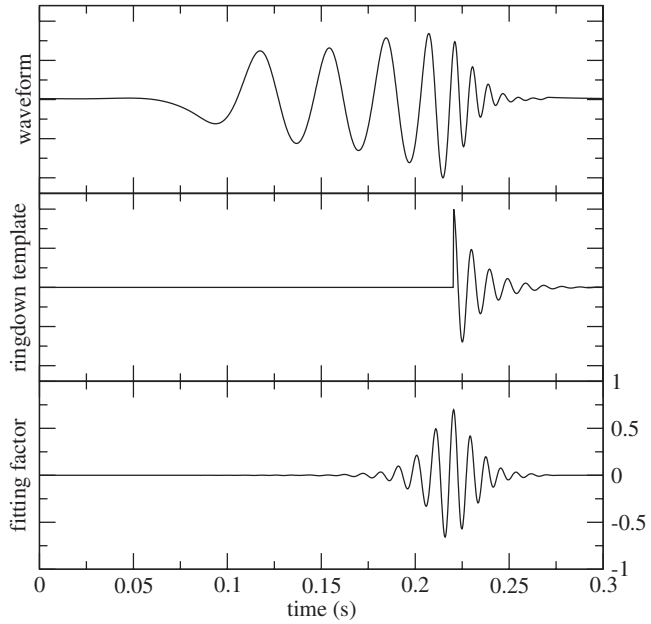

FIG. 10. The h_+ numerical waveform for a total mass of $150M_\odot$ (top), the best-matching ringdown (exponentially damped sinusoid) filter (middle), and the result of filtering the waveform with this filter (bottom), all as functions of time. The match, which is the largest absolute value of the bottom plot, is 70%.

Figures 9 and 10 illustrate the ringdown filter response to the numerical waveforms for two masses, $50M_\odot$ and $150M_\odot$. In these figures there are three panels which show (top) the numerical strain waveform; (middle) the best-matching ringdown template; and (bottom) the result of filtering the waveform with the best-matching ringdown template—the match is the maximum absolute value of this trace. In both cases the match is substantial: 64% for the $50M_\odot$ case and 70% for the $150M_\odot$ case. In the $150M_\odot$ case (Fig. 10) it is clear that the best-matching ringdown filter is in fact matching the ringdown portion of the numerical waveform; however, in the $50M_\odot$ case (Fig. 9), the best-matching ringdown waveform is matching the numerical waveform considerably earlier than the ringdown phase. For the $50M_\odot$ case, the ringdown phase is not in LIGO's sensitive band. The ringdown filter, while it performed reasonably well at detecting the earlier phase of the numerical waveform, could not be used to measure the quasinormal mode frequency of the resulting black hole. Also note that in the $50M_\odot$ case, the match is an overestimate because the numerical waveform is missing a portion of the late inspiral that would be in LIGO's band for this mass, as remarked above.

IV. DISCUSSION AND CONCLUSIONS

Recent computational and algorithmic advances in numerical relativity allow the exploration of strong-field general relativity in regimes which were hitherto inaccessible. In this paper, we have presented a measure of the accuracy of these simulations adapted to the use of these results in observational gravitational-wave astronomy. The formalism presented in Sec. III A is just the match, defined in Ref. [19], applied to waveforms from various numerical simulations. By applying this metric to the equal-mass Cook-Pfeiffer binary black hole simulations presented in [14], we conclude that these simulations show convergence within this measure. Nevertheless, we also sound a cautionary note about the match as used in Sec. III C to measure the convergence: it only measures the convergence, not the physical relevance of the ultimate solution. To determine the latter, one must also examine a host of other issues including the nature of the initial data, the method of waveform extraction, and the commonly examined issues of stability, convergence and independence on boundary effects. Additionally, the currently available waveforms, which cover just a fraction of the relevant sources and analysis similar to those presented here, will need to be carried out as other cases are treated.

In the remainder of this section we conclude by discussing several outstanding issues in the use of numerical relativity as a tool for gravitational-wave astronomy, including faithful extraction of the waveform from the simulations, what could be the most useful information that numerical simulations of compact object interactions could provide in the near-term to enhance the detectability of gravitational waves, and what information from the simulations could help us learn the most about compact objects after detection.

A. Issues in numerical simulations

Numerical simulations carried out by different codes by construction, necessity, and available computational resources adopt different formulations, employ distinct coordinate systems and varied discretization schemes. As a result, care is required not only in translating the results to data analysis, but also in comparing results from different codes. Naturally, concentrating on physical observables, in our particular case gravitational waves, is the sensible way to do this. At the analytical level, a well-defined approach to compute the radiative properties of the spacetime (under natural assumptions) was developed in the 1960's by taking advantage of future null infinity ($\mathscr{I}^+$) [22–24]. However, numerical applications dealing with black hole spacetimes cannot yet reach $\mathscr{I}^+$ (this awaits Cauchy-characteristic matching or the conformal equations to be fully implemented in the type of systems being discussed here) although there is a strong need to compute the radiation produced in the problem. To do so within a numerical simulation, two approaches are routinely taken. One is based on perturbative methods [25–28] which relies on a suitable identification of a background spacetime, in particular, coordinates and extracting specific quantities

from the simulation. A second approach, which has become the most common one, makes use of the infrastructure developed to calculate the radiation at $\mathscr{I}^+$ but applied at a finite distance from the source (see for instance [10,29–35]). While in principle this approach can be used beyond the perturbative level and is less sensitive to identifying a correct background, quantities defined at $\mathscr{I}^+$ need to be translated to finite distances where they may not be well or unambiguously defined.

Several key elements, listed below, are in general required for faithful extraction of gravitational waves a finite distance from the source using the standard result for the relationship between Ψ_4 and the gravitational-wave strain (2) (we focus here on items pertaining to $\mathscr{I}^+$-based extraction tools, though similar comments apply to perturbative-based methods). For the most part in present simulations it is *assumed* that these conditions are satisfied with systematic error less than numerical truncation error—of course, these assumptions will eventually need to be verified, and we discuss some suggestions on how to do this in Appendix A. The items listed below are not all independent. Furthermore, in theory several of the items are *not* strictly required *if* during wave extraction artifacts induced by ''bad'' coordinates are identified and removed; additional discussion of this is also presented in Appendix A.

(i) In the extraction zone the wave travels with unit coordinate velocity, and the amplitude decays as $1/r$. If these conditions are not satisfied the extracted waves could suffer an error in amplitude and a shift in the frequency of the wave (signs of this kind of gauge artifact are seen in the CP evolutions with generalized harmonic gauge [14]).

(ii) The extraction world tube is assumed to be a geometric sphere, and moreover it is assumed that the metric of this sphere can be expressed as $ds^2 = r^2[d\theta^2 + \sin^2\theta d\phi^2]$, where r is the extraction radius and (θ, ϕ) are the usual spherical polar coordinates mapped onto the extraction sphere. Deviations from these assumptions could, for example, lead to artificial mixing of the spherical harmonic components of the waveform; and of course the correct identification of these harmonic components is an important tool in understanding and quantifying the physics of different merger scenarios.

(iii) Each point on the extraction world tube is assumed to correspond to an inertial observer. Together with the above items this is equivalent to assuming that the lapse function $\alpha = 1 + O(1/r)$ and the shift vector induced at the world tube $\beta^A = 0 + O(1/r)$. If these conditions are not satisfied all the problems mentioned in the preceding items could manifest.

(iv) Even with a perfect gauge the $O(1/r)$ approach to Minkowski space could induce spurious effects at finite extraction distance; thus the extraction radius must be far enough from the source that the $O(1/r)$ systematic errors in waveforms are smaller than the numerical truncation error. This issue can be alleviated in part by a judicial choice of the tetrad used to calculate Ψ_4 [33–35].

B. Enhancing the detectability of gravitational waves

Numerical relativity has long been touted as necessary to doing the best science with ground-based gravitational-wave detectors since the strongest sources of gravitational radiation involve strong gravitational fields and the full nonlinearity of general relativity. In [36], Flanagan and Hughes laid out the issues relating to the detection and measurement of waves from binary black holes. They conclude that binary black holes in the mass range $25M_\odot \lesssim M \lesssim 700M_\odot$ may be the strongest sources of gravitational waves accessible to earth-based detectors. In this mass range, they speculated that most of the detectable gravitational-wave energy would come from the merger waves emitted between $f_{\rm isco}$ and $f_{\rm qnr}$ and guessed that about 3% of the binary mass would be emitted as gravitational waves from the ringdown of the final black hole. Numerical relativity simulations can now provide a wealth of information about the merger and ringdown phases of compact binaries, even though precise connection to the inspiral phase may remain elusive for some time.

With the cautionary note that so far numerical simulations have provided input on a (small) subset of the physical parameter space and that, in particular, spin-orbit interactions might strongly influence the modeled waveforms, valuable insights can be drawn with the current knowledge. Consider the simulations of CP initial data discussed here. We can immediately make several qualitative observations about the waves (see also the relevant discussions in [14]). First, the waves sweep smoothly upward in frequency from $f_{\rm isco}$ to $f_{\rm qnr}$; during this phase the time-domain amplitude also increases monotonically. About 3%–5% of the binary mass is radiated in the last plunge-orbit, merger, and ringdown. The analysis in Sec. III E suggests that upwards of ~70% of the wave energy can be attributed to the ringdown waves (though some portion of the wave matched by the ringdown template could be associated with the late-inspiral part of the wave). Perhaps most important for detection of the waves is that the bulk of the wave energy is emitted in a time-frequency volume defined by $102.5(40M_\odot/M) \lesssim f \lesssim 500(40M_\odot/M)$ within a time duration $\Delta t \approx 0.03(M/40M_\odot)$. In the language of Anderson *et al.* [37], the time-frequency volume of the signals is $V = 12$ with a definite mass scaling for the frequency band. Figure 11 compares the sensitivity of a matched filtering search to an excess-power search for several different time-frequency volumes. In the context of these equal-mass, nonspinning binaries, it suggests that a naive excess-power search would miss about half of the signals detectable by a

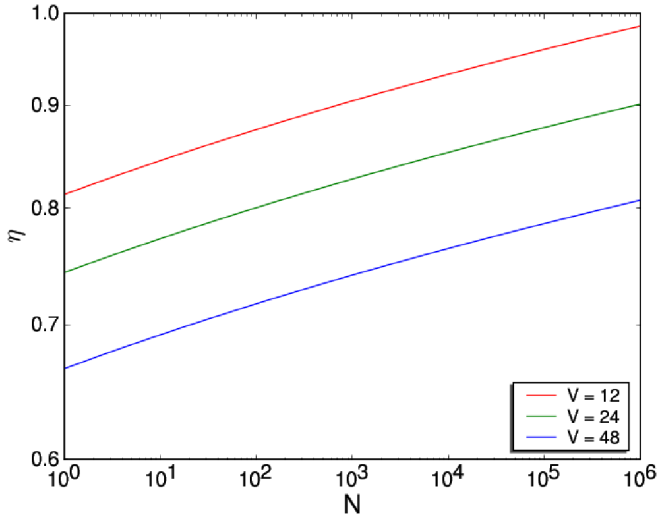

FIG. 11 (color online). The relative effectiveness η of an excess-power search with known time-frequency volume V compared to a matched filtering search with N effectively independent templates assuming both searches are tuned to give a 1% false alarm probability. The relative effectiveness is defined as $\eta = D^{\rm EP}_{99\%}/D^{\rm MF}_{99\%}$ where $D_{99\%}$ is the effective distance at which 99% of the sources are detectable in each search. Given the estimated time-frequency volume of the merger signal from equal-mass binaries, i.e. $V \simeq 12$, this suggests that a suboptimal search strategy could still detect about half the sources that could be detected in a matched filtering search; simple enhancements to the excess-power method should be able to do better. This data is taken from Fig. 4 of Ref. [37].

matched filtering search for the merger only. Nevertheless, this information, when carefully combined with a search for gravitational waves from the inspiral and ringdown phases of binary evolution could provide a near optimal search for these sources.

Dynamical simulations of binary black holes have so far only been carried out for a very limited number of parameters (e.g. mass ratio and black hole spin), and it will be very important to systematically investigate the dependence of the waves on these parameters (compare [15,38]). For example, black hole spin may effect both the amplitude and the duration of the merger waves. For aligned black hole spins the merger takes longer than for antialigned black hole spins [38]. In addition, the interaction between spin and orbital angular momentum may play a role in the dynamics of the merger (even though the speculations of [39] have not been confirmed by the dynamical simulations of [40]).

An important next step in confirming these speculations is to use the waveforms from numerical simulations as sample signals in real detector noise and passed through the current detection pipelines. This would be facilitated by the development of an archive of gravitational waveforms in a uniform format that could be used openly by the gravitational-wave detection community to calibrate their searches and their pipelines. Activities in this direction are already under way [41]; with the intention of developing into a useful resource for gravitational-wave astronomy. As an aside, to expedite their use in data analysis, these waveforms should be provided as an equally sampled time series, with time in units of seconds and scaled to a physical distance of 1 Mpc from the binary.

Despite recent computational and algorithmic advances, numerical simulations are costly and will be for years to come. In Appendix B, we present order of magnitude estimates of the computational cost of simulations needed to produce parameter space surveys of a given accuracy and physical evolution time. This suggests that it will be impossible to populate a template bank solely with the results of numerical simulations in the near to medium term. It is therefore interesting to devise approximate methods which might capture the essential features of the merger phase. One possible approach would be to use PN methods for the early phase and close limit approximations for the late phase with a judiciously chosen behavior in between. Adopting such approximate methods requires a careful understanding of the sensitivity of detection methods to differences in the approximate waveforms.

C. Learning about compact objects through gravitational-wave observations

While the direct observation of gravitational waves will be a huge achievement, we hope that the first detection will only mark the beginning of gravitational-wave astronomy. This field is built on the premise that we can decode information about the sources of gravitational waves from the signals observed at a detector. To achieve this goal, we need the ability to simulate the generation of gravitational waves by various sources. Moreover, it is the imprint of the sources on the waves that will carry some of the most interesting information.

1. Binary black holes

By exploring the results of merger simulations from the perspective of data analysis we can obtain a better picture of what we would be able to learn about compact object interactions from future observations. Therefore it will be very important in the near future to perform surveys of a wide variety of initial data parameters (in particular varying mass ratios and spin vectors), not so much to build template libraries, but to understand what the broad features of merger look like through the lens of a gravitational-wave detector. For example, it has long been anticipated that the onset of the binary merger, at which the slow and adiabatic binary inspiral changes into a dynamical plunge, would occur at an innermost stable circular orbit and would leave a characteristic signature in the gravitational-wave signal, which could be measured in gravitational-wave detectors. While the recent dynami-

cal simulations of binary black holes do not reveal any abrupt change in the waveform, there does appear to be a break in the frequency spectrum of the waves which occurs somewhere between the predicted ISCO frequency and the quasinormal mode frequency—see Fig. 4 and further discussion of this in [14]. It is certainly plausible that this break in frequency becomes more pronounced as one moves away from the equal-mass, nonspinning regime.

Black hole coalescence has also been regarded as giving rise to an arena where the strong-field, nonlinear regime of general relativity will be clearly revealed to observers. The early simulations show perhaps a disappointing lack of such features, where except for a very short and smooth transition between inspiral and ringdown, much of the waveform can be understood using perturbative techniques. Another way of stating this is that all waveforms to date are dominated by the quadrupole harmonic. In general one would expect nonlinear effects to result in mode coupling. Again, that we do not see significant higher order harmonics could be due to the restricted initial conditions so far considered; however, at the very least this is telling us that manifest strong-field effects are not ubiquitous in this type of black hole collisions, and the community will need to search harder to find richer regions of astrophysically relevant parameter space. Whether this observation remains as such in more generic cases will have strong consequences for the simulation and analysis sides. On one hand, deciphering the nonlinear effects would require significantly more accurate simulations and a considerably denser template bank for data analysis. On the other hand, however, these templates could be parametrized in a rather simple form like that in Eq. (18).

2. Binary neutron stars

For binary neutron stars the situation is significantly different from that for binary black holes. Depending on the equation of state, stellar masses and spins, the merger of binary neutron stars may be triggered either by a plunge after the two stars reach an ISCO, or by Roche lobe overflow (see, e.g. [42,43]). In either case, the merger is expected to occur at a gravitational-wave frequency of approximately 2 kHz, outside of LIGO's most sensitive regime. That means that the current LIGO configuration is more sensitive to the inspiral phase, which may be well approximated by post-Newtonian calculations, than the merger of binary neutron stars, which has to be modeled with numerical relativity. Hence, the role of numerical relativity in observing binary neutron stars is different from its role for binary black holes. In the near term, numerical simulations could be used to validate the post-Newtonian approximation to the waveforms in the LIGO frequency band; whether this is possible on current generation computing facilities remains to be seen. Furthermore, numerical relativity may provide guidance for the design of future configurations, given the astrophysical scenarios that seem particularly promising. In the long term, the prospect of observing gravitational radiation from the merger of binary neutron stars is very exciting because it is very rich in physical effects that may play an important role. Unlike binary black holes, which are governed entirely by Einstein's field equations, the dynamical evolution of binary neutron stars also depends on the equation of state, magnetic fields, radiation and neutrino transport, and possibly other effects. Realistic, nuclear equations of state have already been adopted in simulations of binary neutron star mergers [44], and numerical codes that incorporate general relativistic magnetohydrodynamics have been developed (see e.g. [45,46]). Detecting a binary neutron star merger may therefore establish important observational constraints on these aspects, in particular, the equation of state. Clearly, this is a very exciting prospect.

As discussed above, it is unlikely that the current gravitational-wave detectors could observe the details of the merger. Numerical relativity may nevertheless play an important role for the purposes of data analysis, namely, by identifying features in the gravitational-wave signal that could provide particularly important information. A concrete example is the question whether or not the merger remnant promptly collapses to a black hole. Depending on the equation of state, binary neutron stars may either collapse to a black hole on a dynamical time scale after merger or the remnant may form a "hypermassive" neutron star supported against collapse by virtue of differential rotation [44,47]. For binaries with fixed masses the premerger gravitational-wave signal is quite similar, but the post-merger signal differs significantly for the two scenarios. Distinguishing these post-merger signals would therefore provide an important constraint on the neutron star equation of state. Unfortunately, the post-merger signal typically has a frequency close to 4 kHz [44] and may require advanced, perhaps specialized, detectors to extract significant information (see also the discussion in [48]). Investigations of these waves and the information they carry could therefore be used to inform development of advanced gravitational-wave detectors.

3. Black hole-neutron star binaries

For mixed black hole-neutron star binaries the situation is different again. The inspiral can have two very different outcomes: either the neutron star is tidally disrupted by the black hole before it reaches the ISCO, or it reaches the ISCO first and spirals into the black hole more or less intact. A very crude scaling argument suggests that the separation of tidal disruption $s_{\rm tid}$ is approximately

$$\frac{s_{\rm tid}}{M_{\rm BH}} \approx \left(\frac{M_{\rm NS}}{M_{\rm BH}}\right)^{2/3} \frac{R_{\rm NS}}{M_{\rm NS}}, \tag{27}$$

while the ISCO is located approximately at

$$\frac{s_{\rm ISCO}}{M_{\rm BH}} \approx 6. \tag{28}$$

If $s_{\rm tid} > s_{\rm ISCO}$, the neutron star is disrupted before it reaches the ISCO, and vice versa. Since most neutron stars are expected to have a mass of slightly more than a solar mass and ratio $R_{\rm NS}/M_{\rm NS} \approx 5$, the outcome mostly depends on the black hole mass $M_{\rm BH}$ (see Ref. [49]).

The neutron star can only be disrupted tidally outside the ISCO for relatively small stellar-mass black holes with $M_{\rm BH} \lesssim 5M_{\rm NS}$. This regime is very interesting for a number of astrophysical reasons. Such a disruption may act as the central engine of short gamma ray bursts, and, as for binary neutron stars, a detection may provide useful constraints on the equation of state. It is also this regime that requires numerical relativity simulations for quantitative predictions. Extending the above crude estimates, the orbital frequency at the onset of tidal disruption is approximately

$$\Omega_{\rm orb} \approx \left(\frac{M_{\rm BH}}{s_{\rm tid}^3}\right)^{1/2} \approx \left(\frac{M_{\rm NS}}{R_{\rm NS}^3}\right)^{1/2}, \tag{29}$$

which is the same order as the inverse of the neutron star's dynamical time scale. As for the merger of binary neutron stars, the corresponding gravitational-wave frequency is outside of LIGO's most sensitive wave band. The role of numerical relativity is therefore again to explore these scenarios and identify particularly interesting frequency regimes.

Numerical relativity simulations of mixed black hole–neutron star binaries are not as far advanced as those of black hole binaries or neutron star binaries. So far, fully relativistic, self-consistent studies exist for quasiequilibrium models [50–52] (see also [53]). The first fully self-consistent, dynamical simulations of the binary inspiral and the tidal disruption of the neutron star have been announced very recently [54] (see also [55] for simulations of extreme mass-ratio binaries within the so-called Wilson-Mathews approximation, which assumes that the spatial metric remains conformally flat). Other groups have also initiated studies of mixed binaries [56,57]. Clearly, more comprehensive studies of tidal breakup in black hole–neutron star binaries remain an important and urgent goal.

These calculations will help to address several very important questions. One such question is whether the tidal disruption of a neutron star in a mixed binary may lead to an accretion disk that is large enough to power a gamma ray burst. Another question concerns the nature of the mass transfer, which could proceed on a dynamical or secular time scale, or could even be episodal (see, e.g., the discussion in [55] and references therein). The nature of the tidal disruption has great impact on the gravitational-wave signal emitted in the process. Presumably the disruption will leave a signature in the signal at a frequency related to orbital frequency. As inferred from Eq. (29), this frequency carries important information about the neutron star and its structure. A quantitative understanding of these issues clearly requires detailed numerical relativity simulations.

ACKNOWLEDGMENTS

We would like to thank A. Buonanno, G. Cook, O. Moreschi, J. Pullin, and R. Price for helpful discussions. This work was supported in part by NSF Grants No. PHY-0326311 and No. PHY-0554793 to Louisiana State University, No. PHY-0456917 to Bowdoin College, No. PHY-0200852 to University of Milwaukee-Wisconsin, the CIAR, NSERC, and Alberta Ingenuity. The simulations described here were performed on the University of British Columbia's *vnp4* cluster (supported by CFI and BCKDF), *WestGrid* machines (supported by CFI, ASRI, and BCKDF), and the Dell *Lonestar* cluster at the University of Texas in Austin. L. L. thanks CIAR for support to attend the 2005 and 2006 Cosmology & Gravity meetings where portions of this research were started. P. R. B. and L. L are grateful to the Alfred P. Sloan Foundation and Research Corporation for financial support.

APPENDIX A: CALCULATION OF RADIATION AND SYSTEMATIC EFFECTS

In this section we discuss in more detail possible systematic effects resulting in the calculation of waveforms. We concentrate, in particular, in the approach based on the Newman-Penrose (spin-weighted) scalar Ψ_4 as is the most commonly employed; however, similar issues arise in the perturbative approach as well.

1. From the analytical to the numerical arena

Ψ_4 is a particular combination of the Weyl tensor in a suitable frame and coordinates. Its leading order Ψ_4^0 in a suitable Taylor expansion off future null infinity ($\mathscr{I}^+$) provides the gravitational waves. From now on, as we concentrate on the extraction of gravitational waves we will drop the supra-index "0" from all related quantities, though it must be understood that we are referring to the leading behavior. A related quantity, the shear of the outgoing null rays σ plays a crucial role in the calculation of radiated momentum and angular momentum. A few key features are trivially satisfied at $\mathscr{I}^+$ by construction which makes the unambiguous calculation of the radiative properties of the spacetime possible. Namely, the metric is exactly flat, the location of the extraction world tube is unique (up to time u translations), and a powerful structure (like the asymptotic transformation group, asymptotic flatness condition, and peeling behavior) allows for a clean definition of the sought-after quantities. This ensures a unique calculation of the radiative properties of the spacetime.

Unfortunately, most codes are unable to calculate these quantities at future null infinity and thus Ψ_4 is obtained at

finite distances [58]. Since the extraction world tube does not represent a flat surface, key ingredients are missing which can have a nontrivial impact in the calculated quantities, even when the suitable decay of this quantity is materialized (i.e. peeling is satisfied). For instance, the suitable frame allowing for the calculation of radiation at future null infinity—known as a Bondi frame—is such that the angular part of the metric is exactly that of the unit sphere (i.e. the angular metric induced at any given time is exactly that of the unit sphere), there is no induced "shift" in the coordinates of observers at $\mathscr{I}^+$ ($g_{uA} = 0$) and the observers retarded-time u is affinely parametrized ($g_{ur} = 0$). These conditions play a crucial role in several aspects: (i) inertial observers maintain constant angles and clocks that tick at a constant rate, (ii) the variation of the angular part of the metric near $\mathscr{I}^+$ is solely due to gravitational waves, and (iii) the simple relation $\Psi_4 = \bar{\sigma}_{,uu}$ holds (with $\bar{\sigma}$ denoting the complex conjugate of σ). This relation, together with the Bianchi identities at future null infinity, is employed to replace the appearance of $\bar{\sigma}$ by suitable integrals of Ψ_4.

At the numerical level, the world tube is routinely defined by a Cartesian timelike world tube at $x_i^2 = r^2$ intersecting hypersurfaces at $t =$ const. The induced metric on this world tube generically does not satisfy the conditions $g_{AB} = r^2 q_{AB} + O(r)$ (with q_{AB} the unit sphere metric, $g_{tt} = 1$ $g_{tA} = 0$). Consequently, as discussed in detail in [59], if $\Psi_4 \neq \ddot{\bar{\sigma}}$ (with a "$\cdot$" indicating ∂_t), observer's clock rates (at different locations on the extraction world tube) tick at dissimilar rates and do not stay at constant angular locations. These issues can introduce systematic effects which can affect the predicted outcome. For instance,

(i) if $\Psi_4 \neq \ddot{\bar{\sigma}}$, commonly employed formulas which replace $\bar{\sigma}^0$ by integrals of Ψ_4, lack nontrivial contributions from products of $\bar{\sigma}$ and (time derivatives of) the conformal factor F relating the angular metric g_{AB} to the unit sphere metric q_{AB}—see Eq. (A1). Recall that since g_{AB} is the metric of a sphere, it is conformally related to that of the unit sphere by $g_{AB} = r^2 F^2 q_{AB}$

(ii) if $g_{tA} \neq 0$, inertial observers suffer a rotation (from the induced shift $\beta_A = g_{tA}$). Therefore, predictions like the waveforms at a particular angle will be affected as inertial coordinates are shifting around the world tube. This will influence the extraction of multipole contributions, since the spin-weighted spherical harmonics employed in such a task do not take into account the shift in the angular coordinates (see [60] for a related discussion of these issues at $\mathscr{I}^+$).

(iii) if $g_{tt} \neq 1$ the radiation measured by different observers at a constant $t =$ const slice does not correspond to the same inertial time. Thus the extracted waveforms would have to be mapped, at each angle to the real inertial time.

It is clear that these issues can introduce systematic effects that can be either corrected or at least estimated within a given simulation. Notice that these issues cannot be completely addressed with an improved tetrad choice as any tetrad must satisfy $g_{ab} = 2l_{(a}n_{b)} - 2m_{(a}m_{b)}$. Thus, the induced metric in all cases will be the same. Nevertheless a convenient choice of tetrad aids, in particular, to alleviate issues related to the proximity of the extraction world tube to the source.

It is useful to first at least determine the magnitude of the effects the issues discussed above might have in a given simulation. Then, if required, these effects can be corrected by suitably modifying the employed expressions to remove many of the ambiguities. In what follows we describe the first part, while a discussion of the second will be presented elsewhere [59] and applied in relevant scenarios [61].

First and foremost is estimating the amount that the above mentioned effects can have on Ψ_4. We will ignore here those coming due to the extraction at finite distances as a comparison of obtained results at different radii can be employed to estimate this effect. Furthermore, assuming the extraction takes place sufficiently far away, the difference between a derivative in the time labeling the timelike hypersurfaces and null hypersurfaces—beyond gauge factors which we will discuss later—is given by the contribution of spatial derivatives off the extraction world tube times $1/r$ factors due to an approximate "potential" from the source. This effect is also controlled by placing the extraction sphere sufficiently far and comparing the obtained results at different radii. Under these assumptions, the main contribution to the error in assigning the radiation to the straightforwardly calculated Ψ_4 is given by the discrepancy of the extraction sphere being in agreement with that of a Bondi frame. This is made evident by the failure of the induced metric on the sphere to be that of the unit sphere [62]. In turn one has $g_{AB} = r^2 S_{AB}$, which can be reexpressed in terms of $S_{AB} = F(t, \theta, \phi)^2 q_{AB}$ with q_{AB} the unit sphere metric. The correction to Ψ_4 is given by

$$\Psi_4^0 = \ddot{\bar{\sigma}} - \bar{\eth}^2 \frac{\dot{F}}{F} + \bar{\sigma} \frac{\ddot{F}}{F} + 2\left(\dot{\bar{\sigma}} \frac{\dot{F}}{F} - \bar{\sigma} \frac{(\dot{F})^2}{F^2} \right) \qquad \text{(A1)}$$

with $\eth$ the *eth* operator which is a particular combination of derivatives on the sphere [24]. Thus, unless $\dot{F} = 0$, a nontrivial correction must be considered from the fact that the extraction sphere is not inertial. Certainly this will occur as the very radiation one is trying to compute will be responsible for accelerating the sphere. The key message is then to estimate the role F will play. To this end two calculations can be performed. First, a partial answer on the value of F can be obtained by simply evaluating $\tilde{F} = \det(g_{AB})/\det(r^2 q_{AB})$. If $\tilde{F} \neq 1$, then $F \neq 1$ and it can therefore play a nontrivial role. However, if $\tilde{F} = 1$ it is not necessarily the case that $F = 1$. A more involved, though now complete, recipe to obtain F can be easily obtained by computing the Ricci scalar associated with g_{AB}

and q_{AB} and the fact that the two metrics are conformally related by F. This gives rise to the expression $\mathscr{R} = 2(F^2 + \nabla^A \nabla_A \log F)$. Notice that $F = 1$ is a solution if g_{AB} is the unit sphere metric, hence, short of obtaining a solution for F, an estimate of ignoring this fact can be obtained by $\mathscr{E}_F = ||\mathscr{R} - 2||$. Naturally, if $\mathscr{E}_F$ remains well below the measured waveforms, the straightforward use of Ψ_4 would be warranted. To simplify the numerical calculation of $\mathscr{R}$ one can make use of the Gauss-Codacci relations for a two-dimensional hypersurface S in a three-dimensional manifold Σ and employ quantities readily available on Σ. Defining the extrinsic curvature of S by $\kappa_{ab} = h_a^c h_b^d \nabla_c s_d$ (with $h_{ab} = \gamma_{ab} - s_a s_b$, the induced metric on S with normal $\hat{s}_a = \nabla_a R$, $s^a = \hat{s}^a/(\hat{s}_a \hat{s}^a)^{1/2}$ and $\nabla_c \gamma_{ab} = 0$), a straightforward calculation indicates

$$\mathscr{R} = {}^{(3)}R - 2{}^{(3)}R_{ab} s^a s^b - \kappa^2 + \kappa_{cd} \kappa^{cd}. \tag{A2}$$

In addition to the conformal factor F being taken properly into account, a Bondi frame satisfies that observers measure an affine time along $\imath^+$ and proceed along constant angular coordinates. These conditions will be met unless $g_{tt} = 1$, $g_{tA} = 0$. Here again norms could be defined as $\mathcal{E}_{Gtt} = ||(g_{tt} - 1)||$, $\mathcal{E}_{GtA} = ||g_{tA}||$ so as to obtain an estimate of the effect these issues might have in the extraction process.

2. Coordinate conditions and extracted quantities—an example

To illustrate some of the effects of coordinate conditions that are not well adapted to the extraction mechanism, we adopt a spacetime containing linearized gravitational waves [63]. For our particular example, the spacetime is described in terms of the following line element:

$$\begin{aligned} ds^2 = & -dt^2 + (1 + A f_{rr}) dr^2 + 2B f_{r\theta} dr d\theta \\ & + 2B f_{r\phi} \sin(\theta) dr d\phi + (1 + C f^1_{\theta\theta} + A f^2_{\theta\theta}) r^2 d\theta^2 \\ & + 2(A - 2C) f_{\theta\phi} r^2 \sin(\theta)^2 d\theta d\phi \\ & + (1 + C f^1_{\phi\phi} + A f^2_{\phi\phi}) r^2 \sin(\theta)^2 d\phi^2, \end{aligned} \tag{A3}$$

where

$$\begin{aligned} f_{rr} &= \sin(\theta)^2 \cos(2\phi); \qquad f_{r\theta} = \sin(2\theta) \cos(2\phi)/2 \\ f_{r\phi} &= -\sin(\theta) \sin(2\phi); \qquad f_{\theta\phi} = \cos(\theta) \sin(2\phi) \\ f^1_{\theta\theta} &= -f^1_{\phi\phi} = (1 + \cos(\theta)^2) \cos(2\phi) \\ f^2_{\theta\theta} &= -\cos(2\phi); \qquad f^2_{\phi\phi} = -\cos(\theta)^2 \cos(2\phi) \end{aligned}$$

and

$$A = \left(\frac{-3 \sin(Y)}{r^3} + \frac{9 \cos(Y)}{r^4} + \frac{9 \sin(Y)}{r^5} \right), \tag{A4}$$

$$B = \left(\frac{\cos(Y)}{r^2} + \frac{3 \sin(Y)}{r^3} - \frac{6 \cos(Y)}{r^4} - \frac{6 \sin(Y)}{r^5} \right), \tag{A5}$$

$$C = \frac{1}{4} \left(\frac{\sin(Y)}{r} - \frac{2 \cos(Y)}{r^2} - \frac{9 \sin(Y)}{r^3} + \frac{21 \cos(Y)}{r^4} - \frac{21 \sin(Y)}{r^5} \right), \tag{A6}$$

with $Y = t - r$ and for simplicity we have adopted $F = \sin(t - r)$ in Ref. [63]. While a detailed discussion of problematic issues that can arise in the extraction process as well as ways to handle them will be discussed elsewhere [59], we here illustrate the effect that some of these will have in a simple scenario.

Notice that the line element (A3) satisfies all the mentioned properties, in particular $g_{tt} = 1$, $g_{tA} = 0$, and $g_{AB} = r^2 q_{AB} + O(r)$ (with $A = \theta$, ϕ and $q_{AB} = \mathrm{diag}[1, \sin(\theta)^2]$). For clarity, we will concentrate on two very simple cases that will violate these conditions defined by $r \to g(t) r$ and $\phi \to \phi + \omega t$. The former introduces a time-dependent variation in the location of the extraction radius with respect to a physically defined areal radius. The latter induces a shift along the ∂^a_ϕ direction. Following the commonly used approach one obtains for Ψ_4,

$$\Re(\Psi^0_4) = \frac{\sin(\tilde{Y})(1 + \cos(\theta)^2)}{4g} \cos(2(\phi + \omega t)), \tag{A7}$$

$$\Im(\Psi^0_4) = \frac{-\sin(\tilde{Y}) \cos(\theta)}{2g} \sin(2(\phi + \omega t)), \tag{A8}$$

with $\tilde{Y} = t - rg$; clearly, while a calculation of the radiated energy would be immune to the value of ω, the actual waveforms would be affected. Additionally, both would be affected by the functional dependence of $g(t)$, which even when chosen initially to be unity, it will vary as waves propagate outwards affecting the spacetime. Clearly a generic situation would not be as simple as the one analyzed above, though it serves to make evident how these issues can be obscured in a nontrivial extraction of physical quantities in an otherwise correctly obtained numerical solution.

APPENDIX B: ESTIMATING THE COMPUTATIONAL COST OF BINARY BLACK HOLE MERGER SIMULATIONS

Here we present an order of magnitude estimate of the computational cost of simulating a binary black hole merger for a specified number of orbits, and where we want to extract some feature of the solution to within a given accuracy. More precisely, if the CPU run time and estimated net solution error of a fiducial simulation are known, we give an order of magnitude estimate for the CPU run time that a second simulation will take to obtain a new result with the same accuracy but from an evolution that completes a different number of orbits before merger.

Assume the numerical error $E(t, h)$ in some desired property of the solution (for example the phase evolution

of the gravitational waveform) has the following dependence on physical time t and characteristic discretization scale h:

$$E(t, h) \propto t^q h^m. \tag{B1}$$

Here q is a positive constant of order unity, and m is the order of the discretization method. In general the growth of error will be more complicated than this simple power law, though for an order of magnitude estimate this expression is sufficient. Note also that we have assumed the code has been "cured" of any exponential growth in error. In an adaptive code there will be several mesh spacings h, though the scaling relationships derived below will still be correct if all mesh resolutions are changed by the same factor when the resolution is changed. Equation (B1) is strictly only valid for finite-difference codes, though in the final expression below we can take the limit as $m \to \infty$ to get estimates for spectral codes. This will give us an idea of the scaling of present pseudospectral codes in the regime where the leading source of error comes from the spatial discretization and not the finite-difference time stepper.

A more useful parameter describing the physical run time t of the simulation is the number of orbits n completed before coalescence, and we will assume that the inspiral regime of the merger dominates the run time. We can use the leading order post-Newtonian expression for equal-mass, quasicircular inspirals to estimate $n(t)$:

$$n(t) \propto t^{5/8}. \tag{B2}$$

The final ingredient in our scaling estimates will be the manner in which computational run time T scales with mesh spacing h for any *optimal* grid-based solution method of a 3 + 1-dimensional system of partial differential equations

$$T(h, t) \propto \frac{t}{h^4}. \tag{B3}$$

The first question we can now answer is the following: given that simulation A required T_A CPU hours to complete a simulation of a binary system exhibiting n_A orbits before coalescence, and from which we extracted a desired quantity with error E_A, how long T_B will it take to run a second simulation of a similar binary system, now with n_B orbits before coalescence but the *same* net error $E_B = E_A$? Using (B1)–(B3) we find

$$T_B = T_A \left(\frac{n_B}{n_A}\right)^{(8/5+32q/5m)}. \tag{B4}$$

For example, assuming linear growth of error ($q = 1$), we get $T_B = T_A^z$, where $z = 4.8, 3.2, 2.7, 2.4, \ldots, 1.6$ for $m = 2, 4, 6, 8, \ldots, \infty$, respectively. Note that the difference going from 2nd to 4th order accuracy is quite significant, as is the jump from 4th to "spectral" convergence $m = \infty$. The same holds when estimating the accuracy achieved by different order-of-accuracy operators in modeling modes in the solution [64,65]. This implies that while higher order methods are important, a significant gain is already achieved at 4th order.

An application of the preceding expression is to the recent survey of unequal mass inspirals presented in [9]. The 4th order accurate code ($m = 4$) discussed there is quite fast by today's standards, and they were able to perform the survey utilizing a total of about 150 000 CPU hours (recall however that the cost of these simulations is in practice further alleviated by exploiting the problem's symmetry). The majority of initial conditions ran exhibited about 2 orbits before merger. Suppose the survey were repeated (including calibration runs, etc.), but now starting with initial conditions resulting in 4 orbits prior to merger. Equation (B4) suggests (assuming $q = 1$) it would take around 1.4×10^6 CPU hours to complete with the same level of overall accuracy. Early comparisons of numerical versus PN waveforms [14] suggest more than 4 orbits are needed to begin to study the adequacy of various PN approximants. Suppose 10 were sufficient, and the survey of [9] were repeated for the purpose of PN comparisons—(B4) then suggests 170×10^6 CPU hours would be needed. This would require a 20 000 node cluster running continuously for 1 year. Of course, we are *not* suggesting that such a survey is necessary for PN comparison purposes, we are merely illustrating (B4) using actual data for the reference simulation "A" as given in [9].

A second interesting question we can give a rough answer to is, Given simulation A has accumulated an error E_A for an n_A orbit simulation, what is the expected error for simulation B that completes n_B orbits, assuming simulations A and B have identical resolution $h_A = h_B$?

$$E_B = E_A \left(\frac{n_B}{n_A}\right)^{(8q/5)}. \tag{B5}$$

At a first glance it might seem strange that the accumulation of error is independent of the order of the discretization scheme. Although, observe that this does *not* imply that a lower order scheme is just as "fast" as a high order method even if both methods exhibit similar growth factors q, for in general it will take more resolution for a low order method to get to the same level of error E as a higher order method. From (B3) the ratio of run times T_{h_1}/T_{h_2} for two different resolutions h_1 and h_2, regardless of the order of convergence for an optimal solution method, scales as $(h_1/h_2)^4$.

[1] B. Abbott *et al.* (LIGO Scientific Collaboration), Phys. Rev. D **73**, 102002 (2006); **72**, 082002 (2005); **72**, 082001 (2005).

[2] B. Abbott *et al.* (LIGO Scientific Collaboration), Phys. Rev. D **73**, 062001 (2006).

[3] V. Wainstein and V. Zubakov *Extraction of Signals from Noise* (Prentice-Hall, London 1962).

[4] F. Pretorius, Phys. Rev. Lett. **95**, 121101 (2005).

[5] J. Baker, J. Centrella, D. Choi, M. Koppitz, and J. van Meter, Phys. Rev. Lett. **96**, 111102 (2006).

[6] M. Campanelli, C. O. Lousto, P. Marronetti, and Y. Zlochower, Phys. Lett. **96**, 111101 (2006).

[7] F. Herrmann, D. Shoemaker, and P. Laguna, arXiv:gr-qc/0601026.

[8] U. Sperhake, Phys. Rev. D **76**, 104015 (2007).

[9] J. A. Gonzalez, U. Sperhake, B. Bruegmann, M. Hannam, and S. Husa, Phys. Rev. Lett. **98**, 091101 (2007).

[10] B. Bruegmann, J. A. Gonzalez, M. Hannam, S. Husa, U. Sperhake, and W. Tichy, Phys. Rev. D **77**, 024027 (2008).

[11] G. B. Cook and H. P. Pfeiffer, Phys. Rev. D **70**, 104016 (2004).

[12] I. P. Pfeiffer, http://www.tapir.caltech.edu/~harald/PublicID/.

[13] H. P. Pfeiffer, L. E. Kidder, M. S. Scheel, and S. A. Teukolsky, Comput. Phys. Commun. **152**, 253 (2003).

[14] A. Buonanno, G. B. Cook, and F. Pretorius, Phys. Rev. D **75**, 124018 (2007).

[15] F. Pretorius, Classical Quantum Gravity **23**, S529 (2006).

[16] J. G. Baker, J. M. Campanelli, and F. Pretorius as presented at the New Frontiers in Numerical Relativity Workshop, Golm (2006).

[17] P. Laguna as presented at the Numerical Relativity and Data Analysis meeting, Boston (2006).

[18] L. E. Kidder, C. M. Will, and A. G. Wiseman, Phys. Rev. D **47**, R4183 (1993).

[19] B. J. Owen, Phys. Rev. D **53**, 6749 (1996).

[20] T. A. Apostolatos, Phys. Rev. D **52**, 605 (1995).

[21] Related metrics have been discussed recently to estimate the needed accuracy of the simulated waveforms and remove numerical errors as well as computational grid effects [69].

[22] H. Bondi, M. van der Burg, and A. Metzner, Proc. R. Soc. A **269**, 21 (1962).

[23] R. Sachs, Proc. R. Soc. A **270**, 103 (1962).

[24] E. T. Newman and R. Penrose, J. Math. Phys. (N.Y.) **3**, 566 (1962).

[25] T. Regge and J. A. Wheeler, Phys. Rev. **108**, 1063 (1957).

[26] F. Zerilli, Phys. Rev. Lett. **24**, 737 (1970).

[27] V. Moncrief, Ann. Phys. (N.Y.) **88**, 323 (1974).

[28] A. M. Abrahams and R. H. Price, Phys. Rev. D **53**, 1963 (1996).

[29] S. A. Teukolsky, Astrophys. J. **185**, 635 (1973).

[30] L. Smarr, in *Sources of Gravitational Radiation*, edited by L. Smarr (Cambridge University Press, Cambridge, England, 1978).

[31] J. G. Baker, M. Campanelli, and C. O. Lousto, Phys. Rev. D **65**, 044001 (2002).

[32] M. Campanelli, B. J. Kelly, and C. O. Lousto, Phys. Rev. D **73**, 064005 (2006).

[33] C. Beetle, M. Bruni, L. M. Burko, and A. Nerozzi, Phys. Rev. D **72**, 024013 (2005).

[34] A. Nerozzi, C. Beetle, M. Bruni, L. M. Burko, and Denis Pollney, Phys. Rev. D **72**, 024014 (2005).

[35] A. Nerozzi, M. Bruni, V. Re, and L. M. Burko, Phys. Rev. D **73**, 044020 (2006).

[36] E. E. Flanagan and S. A. Hughes, Phys. Rev. D **57**, 4566 (1998).

[37] W. G. Anderson, P. R. Brady, J. D. E. Creighton, and E. E. Flanagan, Phys. Rev. D **63**, 042003 (2001).

[38] M. Campanelli, C. O. Lousto, and Y. Zlochower, Phys. Rev. D **74**, 041501 (2006).

[39] R. H. Price and J. T. Whelan, Phys. Rev. Lett. **87**, 231101 (2001).

[40] M. Campanelli, C. O. Lousto, and Y. Zlochower, Phys. Rev. D **74**, 084023 (2006).

[41] Collaboration sites for the exchange of numerical relativity waveforms exist at https://astrophysics.gsfc.nasa.gov/GW-Exchangewiki and https://gravity.psu.edu/wiki_NRwaves.

[42] K. Uryū, M. Shibata, and Y. Eriguchi, Phys. Rev. D **62**, 104015 (2000).

[43] K. Taniguchi and E. Gourgoulhon, Phys. Rev. D **68**, 124025 (2003).

[44] M. Shibata and K. Taniguchi, Phys. Rev. D **73**, 064027 (2006).

[45] M. D. Duez, Y. T. Liu, S. L. Shapiro, M. Shibata, and B. C. Stephens, Phys. Rev. D **73**, 104015 (2006).

[46] M. Anderson, E. Hirschmann, S. Liebling, L. Lehner, D. Neilsen, and I. Olabarrieta (unpublished).

[47] T. W. Baumgarte, S. L. Shapiro, and M. Shibata, Astrophys. J. Lett. **528**, L29 (2000).

[48] A. Lewis, T. W. Baumgarte, and P. Brady (unpublished).

[49] M. Vallisneri, Phys. Rev. Lett. **84**, 3519 (2000).

[50] T. W. Baumgarte, M. L. Skoge, and S. L. Shapiro, Phys. Rev. D **70**, 064040 (2004).

[51] K. Taniguchi, T. W. Baumgarte, J. A. Faber, and S. L. Shapiro, Phys. Rev. D **74**, 041502(R) (2006).

[52] P. Grandclement, Phys. Rev. D **74**, 124002 (2006); **75**, 129903 (2007).

[53] M. A. Miller, arXiv:gr-qc/0106017.

[54] M. Shibata and K. Uryū, arXiv:astro//0611522.

[55] J. A. Faber, T. W. Baumgarte, S. L. Shapiro, K. Taniguchi, and F. A. Rasio, Phys. Rev. D **73**, 024012 (2006).

[56] N. T. Bishop, R. Gomez, L. Lehner, M. Maharaj, and J. Winicour, Phys. Rev. D **72**, 024002 (2005).

[57] F. Loffler, L. Rezzolla, and M. Ansorg, Phys. Rev. D **74**, 104018 (2006).

[58] Notable exceptions are provided by implementations based on the characteristic and conformal formulations of general relativity (see [70,71] and references therein). However, these approaches have not yet been used to tackle binary spacetimes of the types discussed here.

[59] L. Lehner and O. Moreschi, Phys. Rev. D **76**, 124040 (2007).

[60] N. T. Bishop, R. Gomez, L. Lehner, M. Maharaj, and J. Winicour, Phys. Rev. D **56**, 6298 (1997).

[61] M. Anderson, L. Lehner, I. Olabarrieta, and C. Palenzuela (unpublished).

[62] J. Winicour, Gen. Relativ. Gravit. **19**, 281 (1987).

[63] S. Teukolsky, Phys. Rev. D **26**, 745 (1982).
[64] L. Lehner, S. L. Liebling, and O. Reula, Classical Quantum Gravity **23**, S421 (2006).
[65] J. Ray, C. A. Kennedy, S. Lefanty, and H. N. Najm, Proceedings of the Third Joint Meeting of the U.S. Section of the Combustions Institute (2003).
[66] LIGO Scientific Collaboration, Report No. LIGO-G060293-01-Z (http://www.ligo.caltech.edu/docs/G/G060293-02/).
[67] L. Blanchet, B. R. Iyer, C. M. Will, and A. G. Wiseman, Classical Quantum Gravity **13**, 575 (1996).
[68] Saikat Ray-Majumder, PhD thesis, University of Wisconsin-Milwaukee, 2006.
[69] M. A. Miller, Phys. Rev. D **71**, 104016 (2005).
[70] H. Friedrich, Lect. Notes Phys. **604**, 1 (2002).
[71] J. Winicour, Living Rev. Relativity **8**, 10 (2005).